Effects of Reduced Gravity on Nucleate Boiling Bubble Dynamics in Saturated Water

R. SIEGEL and E. G. KESHOCK

Lewis Research Center, Cleveland, Ohio

A study was made of nucleate boiling bubble dynamics in saturated distilled water for various reduced gravity fields. The nucleation occurred on a very smooth horizontal nickel surface at low heat fluxes. Since because of the smooth surface finish only a few nucleation sites were active, it was possible to photograph individual bubbles that were not interfered with by adjacent bubble columns. Data were taken at seven different gravity fields in the range from 1.4 to 100% of earth gravity by placing the apparatus on a counterweighted falling platform. Measurements were made of bubble departure diameters and frequencies, growth rates, contact angles, base circle diameters, and rise velocities. Comparisons were made to determine whether the measured gravity dependence of these quantities was in agreement with that predicted by correlations in the literature.

In the design of systems for space applications the effects of reduced gravity fields must often be considered. In an orbiting satellite or in space distant from planetary bodies the gravity field will closely approach zero. In a system that is accelerating slightly, or on bodies such as the moon, the gravity field will be a fraction of that on earth. Heat transfer processes such as pool boiling, condensation, and free convection are gravity dependent and hence would be expected to behave differently in reduced gravity fields. The effect of gravity has been indicated in numerous theoretical and experimental heat transfer correlations by the presence of a g factor. Although a number of experiments have been conducted to study high-gravity effects (*1* to *4*), there has been relatively little experimental work investigating the functional form of the g dependence in the reduced gravity range.

The present paper is concerned with bubble dynamics for saturated pool boiling in reduced gravity fields in the range from 1.4 to 100% of earth gravity. A previous paper (*5*), concerned mainly with burnout for low-gravity conditions, gives some information on bubble rise velocities and bubble diameters at departure for boiling water. It was found that the departure diameters increased as $g^{-2/7}$ rather than $g^{-1/2}$, as is commonly indicated in correlations such as the Fritz equation (reference *12*). In the present study an improved apparatus was used which permitted studies of bubble dynamics in greater detail. In (*5*) the nickel ribbon used as a test surface was generally quite crowded with nucleation sites, and bubbles probably interfered with each other. Consequently the diameters measured at bubble departure were likely not those of single bubbles grown from a single nucleation site without interference from adjacent bubbles. Also the nickel ribbon in (*5*) was only 0.2 in. wide, and hence the bubbles may have had a tendency to grow asymmetrically, that is elongated in the direction along the ribbon length. This would be especially true under reduced gravity conditions, where the bubbles can become quite large for boiling water.

In the present apparatus boiling took place from a flat, horizontal circular area ⅞ in. in diameter. This permitted the bubbles to grow in all directions with equal case. The test surface was given a very smooth, mirrorlike finish, which greatly reduced the bubble population in the low heat flux range. This permitted the detailed observation of bubbles growing from a single site that were not interfered with by adjacent bubble columns, a condition not readily obtainable when ordinary engineering surfaces are used. Since the theoretical predictions of bubble behavior generally deal with isolated bubbles, the intent was to obtain these idealized conditions experimentally in order to provide meaningful comparisons with theory.

Measurements in reduced gravity fields should provide some insight into determining which theoretical predictions and experimental correlations are most general. For example in (*6*) a correlation is briefly mentioned where the diameter of a departing bubble varies as $g^{-1/3}$ rather than $g^{-1/2}$ as in the Fritz equation (reference *12*), and differences of this type remain to be resolved. In departure theory a correction accounting for the bubble growth rate or the inertia associated with the bubble is generally neglected for normal gravity fields except in a few references such as (*7*) and (*8*). However at low gravities the total buoyancy force on a bubble may become very small; hence the effect of inertia may become more significant.

EXPERIMENTAL APPARATUS

Counterweighted Drop Tower

A drop tower with an adjustable counterweight was used to obtain seven gravity fields ranging from 1.4 to 100% of earth gravity. A simplified diagram of the tower is shown in Figure 1*a* and is a refinement of the apparatus used in (*5*) and (*9*). The boiling experiment was mounted on an aluminum platform that could be dropped 12.5 ft. before being decelerated by virtue of vertical pipes mounted underneath the platform penetrating into a sand bed. During deceleration the counterweights are brought to a stop by a friction brake mounted on the counterweight holder. The platform was centered between vertical rails by eight soft rubber wheels, which were in light contact with the rails and rotated freely on bearings. No attempt was made to overcome all the friction in the system which would be required for studying zero-gravity conditions.

Before data were taken, the rate of descent of the platform corresponding to various counterweight loadings was measured so that the effective gravity field on the platform would be known. A vertical measuring scale was fastened to the wall adjacent to the drop tower. For various counterweight sizes the scale was photographed as the platform descended. The change of distance ΔS was read from the film for each time interval Δt as recorded by timing marks on the film margin. A plot of $\Delta S/\Delta t$ as a function of t was then made, and the data gave a well-defined straight line for each counterweight size. The slope of this line was the platform acceleration, and earth gravity minus this acceleration gave the effective gravity field in which the boiling was taking place.

Test Boiler

The boiler construction is illustrated in Figure 1*b*. The boiling test surface is at the end of a ⅞-in. diam. copper rod, the

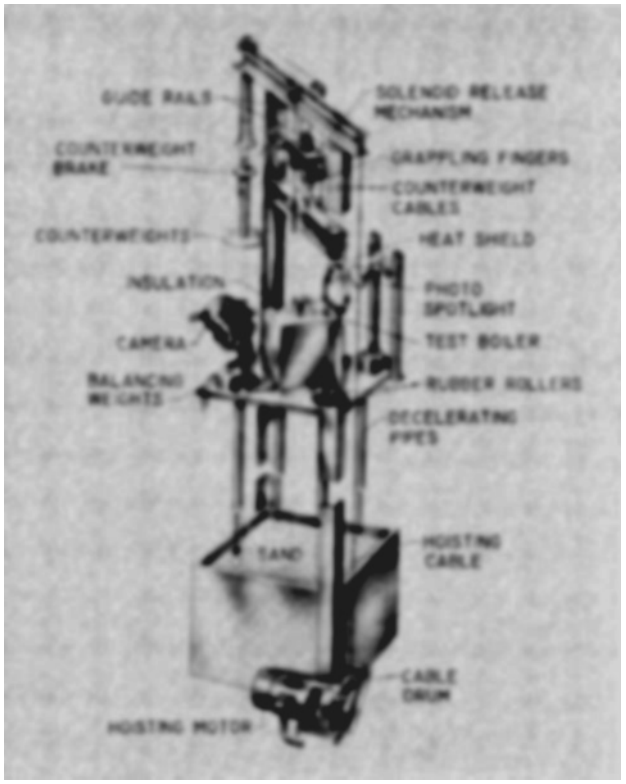

Fig. 1*a*. Experimental apparatus. Counterweighted drop tower (total height, 22.5 ft.).

base of which is heated by two 500-w. cartridge heaters. The circular boiling area is surrounded by a thin fin 0.020 in. thick, which is an integral part of the rod. The entire piece was machined from a single large rod in order to prevent any boiling from cracks that might have developed at the junction between the rod and fin had they been two separate pieces. The fin attenuates the surface temperature so that boiling does not occur from the fin area or from the O-ring joint around the outside of the fin. This prevents bubbles from rising in the foreground, which would obscure photographing the test area.

To limit the number of natural nucleation sites the surface was carefully prepared by lapping and polishing it to a 4-μ in. root-mean-square roughness. Then it was given a thin nickel plating (about 0.0005 in.) and finally polished with a paste of water and very fine alumina. The final polishing was repeated before each use of the boiler. With these surface conditions and a low heat flux it was possible to obtain only one or two nucleating bubble columns on the test area.

Two 250-w. cartridge heaters were mounted in copper fins extending through the top of the boiler into the pool of water. The fins kept the fluid at the saturation temperature.

The boiler was mounted in a plywood box filled with powdered insulation. Only the test surface and glass enclosure were left exposed.

Instrumentation

As shown in Figure 1*b* iron-constantan thermocouples were mounted in 0.030-in. holes at several positions along the axial length of the copper rod. Successive holes were spaced 90 deg. apart around the periphery to provide as little interference as possible with the symmetry of the axial flow of heat. The thermocouple measurements gave the temperature gradient along the rod from which the heat flux could be evaluated. The temperature distribution was extrapolated to give the surface temperature.

Photographs were taken with a 16-mm. motion picture camera at about 3,500 frames/sec. Lens extension tubes were used to magnify the field: generally an area about 1 by ¾ in. was photographed. It was not desirable to use too great a magnification as the bubbles in low-gravity fields can become so large that they grow out of the field of view. A 500-cycle sq.-wave generator was used to place timing marks on the film every one-thousandth of a second.

Illumination was provided by a single 750-w. photo spotlight mounted about 5 in. above and 15 in. to the rear of the test surface. This type of backlighting was found to give good contrast so that the bubble outlines were clearly defined. A flat circular cell containing ½ in. of water between two pieces of plate glass was placed between the light and the boiler. This absorbed most of the heat from the light, and thus thermal equilibrium was not disturbed when the light was turned on.

The fluid temperature was measured with two thermocouples each mounted inside a stainless steel tube 0.0625 in. in diameter. One of the tubes was extended into the photographic field to provide a standard of size for calibrating the bubble measurements.

Experimental Procedure

The method of operation can be conveniently described by discussing a typical experimental run. The test surface was cleaned, polished, and wiped with tissue and distilled water, and the boiler was then assembled and filled with water. The upper heating fins were turned on to bring the water to the saturation temperature and drive off dissolved gases. The test section was heated slowly in order to activate only a few nucleation sites. The water was boiled for a few hours to achieve a steady state condition and for deaeration. If the number of active sites was excessive, this procedure was repeated until a situation was obtained where a steady stream of bubbles issued from only one or two sites.

The platform was raised into position and the counterweight loading adjusted to provide the desired gravity field. The photographic light was turned on, and a switch was then closed which simultaneously started the camera and timer. After a preset time interval (usually about ¼ sec.) the timer activated a solenoid release which dropped the platform. As soon as the platform started to move, it energized a microswitch in the pulse generator circuit which placed a light flash on the film margin to identify the beginning of the reduced gravity period. By providing a time delay before releasing the platform the first part of each film recorded nucleation under normal gravity conditions so that comparisons could be made with the reduced gravity period immediately following. The counterweight was then adjusted to provide another gravity

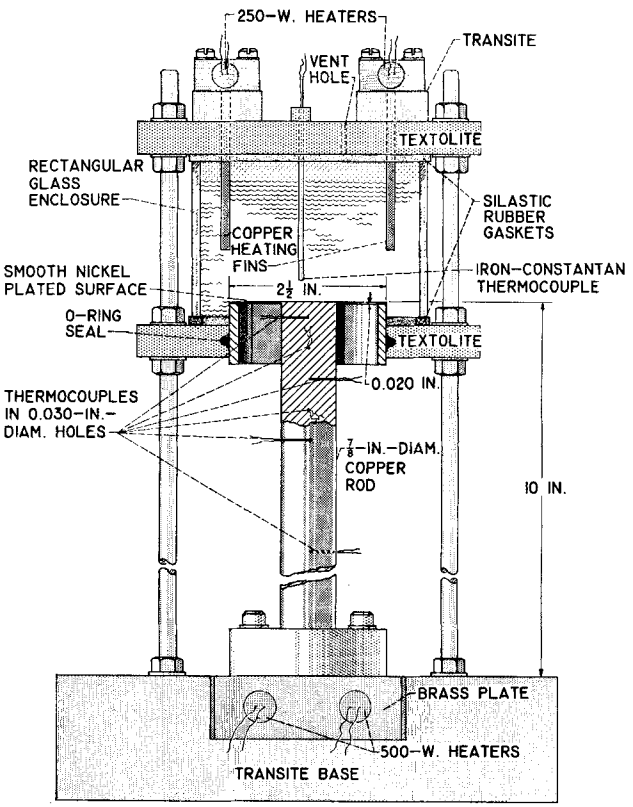

Fig. 1*b*. Experimental apparatus. Test boiler assembly.

field and the runs continued until the same nucleation site had been photographed in all the different gravity fields. Two or three 100-ft. rolls of film were taken for each site at each gravity field.

Measurements were obtained by viewing the films on a motion analyzer which projected a magnified image on a ground glass screen. To obtain the best possible comparisons with theory, measurements were made only on bubbles growing from single nucleation sites. In some instances, after a bubble was partially grown, other nucleation sites would be initiated near the bubble base, and this would cause small bubbles to merge with the original bubble. Measurements were not made for this type of bubble.

RESULTS AND DISCUSSION

The experimental results will now be presented and compared with some of the theories given in the literature. Each subsection will deal with a different aspect of the bubble dynamics. The theory will be reviewed, and then comparisons will be made with the experimental results.

Test Conditions

Because each test run was only about 1 sec. in duration a discussion of transient considerations is warranted. The runs were initiated from a steady state condition at normal gravity, and hence the heat flux and surface temperature are initially at an equilibrium condition corresponding to 1 g_n. The duration of the reduced gravity period is sufficiently short, so that when one considers the high thermal capacity of the heating plate, the temperature distribution

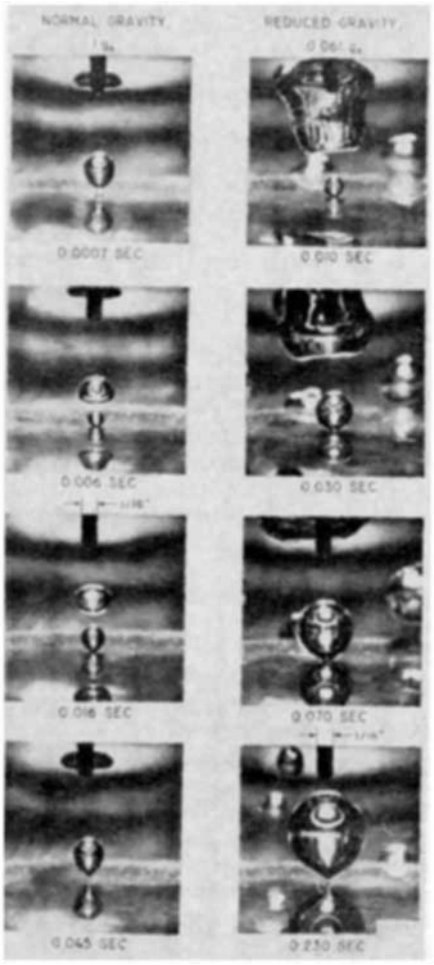

Fig 2a. Comparison of bubbles growing in normal gravity and 6.1% of normal gravity for site 2. Time is measured from onset of growth for each bubble. (The black vertical probe at the top of each picture is 1/16 in. wide.)

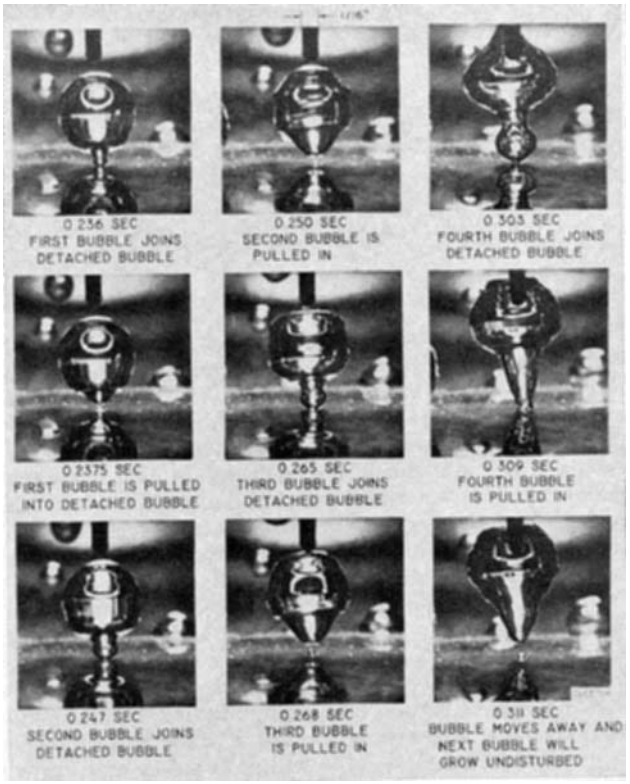

Fig. 2b. This is a continuation of the growth of reduced gravity (0.061 g_n) bubble if Figure 2a. It shows the merging of successive bubbles with undisturbed bubble in Figure 2a.

of the test surface probably does not change appreciably. Hence during the test the conditions are probably not identical to those for equilibrium at low gravity. However in (5) measurements for nucleate boiling in reduced gravity indicated that the curve of q against $T_w - T_{sat}$ depends only slightly on gravity in the reduced gravity range. Hence the present tests may be close to equilibrium as far as these quantities are concerned.

Another factor which may be of some influence is the convection pattern which is present during the initial period of normal gravity boiling. These currents may retain their original identity to some extent and influence the bubble motion in the reduced gravity period.

A third consideration is the temperature distribution in the fluid layer near the surface. For boiling in normal gravity there is a thin layer of superheated liquid near the surface. For low surface heat fluxes the thickness of this layer is partially governed by free convection, and hence it would be expected that the layer thickness would increase when gravity is reduced. The analysis in (10) can be used to provide a rough indication of the transient time required to establish a free convection boundary layer. This indicates that if a heat flux is suddenly applied to a plate in reduced gravity, the transient time varies as $1/(g/g_n)^{0.4}$ and hence can become large when g becomes very small. For the heat flux range in these studies ($q \sim$ 11,000 to 18,000 B.t.u./hr. sq. ft.) and $g/g_n = 0.1$ the transient time for a plate with a characteristic length of 1 in. is about 3 sec. Hence some transient effects may be present in the liquid at the lower gravities and should be kept in mind when evaluating the present work. It would be desirable to have longer periods of reduced gravity, but this is difficult because of the large height required for the counterweighted drop tower.

Nucleation Cycle and Coalescence of Successive Bubbles in Reduced Gravity

As the gravity field is reduced, the detached bubbles begin to rise very slowly because of decreased buoyancy.

Table 1. Heat Fluxes and Temperature Differences During Different Test Runs

Site	q, B.t.u./(hr.)(sq. ft.)	$T_w - T_{sat}$, °F.
1	10,900	11.1
2	17,700	17.0
3	12,700	12.4
4	12,700	12.4

This leads to a bubble coalescence mechanism that is much less frequently observed during normal gravity boiling. (Photographs of a typical normal gravity nucleation cycle are shown in Figure 2*a*.) After a bubble departs and begins to move upward, if its rise velocity is small, the next bubble growing at the surface will collide with it because of the rapid rate at which the bubble diameter increases during the early stages of growth. When the gravity field is only a few percent of normal gravity, a bubble will detach and then remain close to the surface for perhaps 0.1 sec. During this time the bubbles formed at the nucleation site will contact the detached bubble and merge with it, thereby being pulled from the surface before they can grow very large. This is illustrated by the sequence of photographs in Figure 2*b*. Several bubbles will rapidly feed into the larger bubble until it finally rises out of range. Then the next bubble will grow in an undisturbed manner.

The low-gravity boiling regime is thus characterized by a distinctive cyclical behavior. An undisturbed bubble will grow to its final size and detach in a normal manner. Then several small bubbles will pump into it before it can rise away from the surface. The large bubble thus serves as a temporary vapor sink near the surface and absorbs the new bubbles while they are relatively very small. The bubble frequency is quite high when the small bubbles are pumping into the larger one. This could greatly increase the turbulence induced near the surface, which would promote a high heat transfer coefficient. Hence this portion of the bubble cycle could play an important role in reduced gravity boiling heat transfer. At higher heat fluxes there will be many nucleation sites, and a bubble will generally not have the opportunity to grow to completion without interference from adjacent bubbles. In this case the boiling process could be largely dependent on the small bubbles which form and rapidly merge with a vapor mass remaining near the heated surface.

Diameter of Bubbles at Departure

Theoretical relations. Several theoretical relations have been proposed for predicting the size of bubbles at departure from a horizontal surface, and some of these will now be reviewed. The best known is the Fritz (*12*) equation

$$D_d = 0.0208\,\theta \left[\frac{\sigma_{lv}}{g(\rho_l - \rho_v)}\right]^{1/2} \quad (1)$$

where the contact angle θ is in degrees. A relation by Zuber (*6*) is

$$D_d = \left[\frac{6\sigma_{lv}}{g(\rho_l - \rho_v)}\,\frac{k\,\Delta T}{q}\right]^{1/3} \quad (2)$$

A correlation given by Staniszewski (*8*) is

$$D_d = 0.0071\,\theta \sqrt{\frac{2\sigma_{lv}}{g(\rho_l - \rho_v)}}\left[1 + 0.435\left(\frac{dD}{dt}\right)_d\right] \quad (3)$$

where dD/dt is in inches per second. Cole (*13*) gives the equation

$$D_d = 0.040\,\theta \left[\frac{\sigma_{lv}}{g(\rho_l - \rho_v)}\right]^{1/2}\left[\frac{g\sigma_{lv}}{u_d^4(\rho_l - \rho_v)}\right]^{-0.22} \quad (4)$$

Experimental measurements. The diameters of single bubbles were measured at the instant they broke away from the surface. The height and width of a bubble were measured at departure, and the average of these measurements was used as the diameter. In the normal gravity portion at the beginning of each film roll there were generally about ten bubbles that were not interfered with. For each film roll an arithmetic average diameter was computed for these bubbles and is given in the columns labeled N (normal gravity) in Table 2 (a)* for four different nucleation sites. For each site the values in the N columns were averaged to give a final average for the normal gravity condition, and these values are listed in the column labeled $D_{d,n}$. All data for each site were obtained from the same fixed ebullient location which remained active throughout the low gravity and deceleration periods.

As the gravity fields were progressively reduced, the bubbles become much larger and had considerably longer growth times. At several percent of normal gravity only two or three bubble histories could be photographed on a roll of film, while for 0.429 g_n there were about twenty bubble histories. Hence the average values given in the columns labeled R (reduced gravity) in Table 2(a) have a greater statistical weight in the higher gravity range. For 0.014 g_n the growth time was approximately equal to the length of the test run; hence only a small amount of data was obtained because of the difficulty of obtaining a complete history for a bubble that had not been interfered with during its growth.

Comparisons for normal gravity. First consider how well the theoretical equations predict the departure diameters for normal gravity. The comparisons for sites 1 and 2 are given as follows:

	Experimental			Computed $D_{d,n}$, in.		
Site	$D_{d,n}$, in.	θ, deg.	$(dD/dt)_{d,n}$, in./sec.	Equation (1)	Equation (2)	Equation (3)
1	0.093	38	1.0	0.078	0.065	0.054
2	0.134	47	1.0	0.096	0.064	0.067

The q and ΔT used in Equation (2) are given in Table 1. The values of $(dD/dt)_d$ for Equation (3) have been taken from growth rate curves for typical bubbles from sites 1 and 2 (as in Figure 5*a*) and are approximate average values. All of the predicted diameters are too low, and the best results are given by Equation (1), although it provides values that are still about 20% too low. A possible reason for this is that expressions such as Equations (1) and (2) are derived for static conditions by equating the buoyancy and adhesion forces. However for an actual bubble it takes a finite time for the vapor column at the bubble base to collapse and for detachment to occur. During this time the bubble can grow an additional amount. No results were computed from Equation (4) because it was not possible to determine accurately the magnitude of u_d, the bubble rise velocity at departure.

Comparisons for reduced gravity. The variation of bubble diameters as a function of the fraction of normal gravity g/g_n is given in Figure 3. Each data point corresponds to the average departure diameter at a particular site and reduced gravity, divided by the average of all the normal gravity data taken at that site. Equation (1) contains both a gravity factor and the contact angle at departure. The data in Figure 6 (and in Table 3) indicate that for a particular nucleation site the contact angle does not de-

* Tables 2, 3, and 4 have been deposited as document 7969 with the American Documentation Institute Photoduplication Service, Library of Congress, Washington 25, D. C., and may be obtained for $1.25 for photoprints or 35-mm. microfilm.

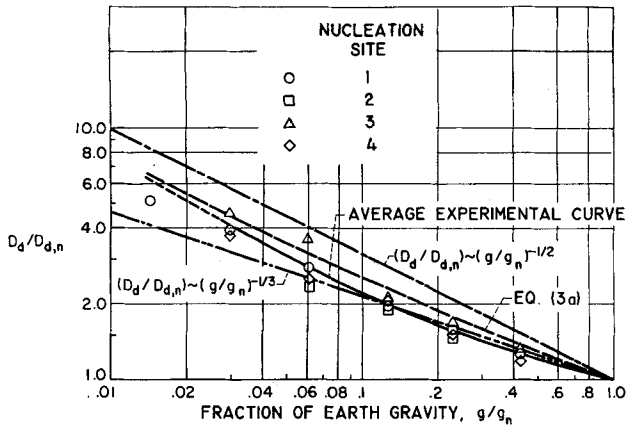

Fig. 3. Effect of reduced gravity on diameters of single undisturbed bubbles at instant of detachment from surface.

pend significantly on g. Hence Equation (1) predicts $D_d \sim g^{-1/2}$, which is the trend of the data in Figure 3 for g/g_n less than about 0.1. For $g/g_n > 0.1$ the trend is more like $g/g_n^{-1/3}$, as indicated by Equation (2). Equation (3) has a dynamic growth factor $(dD/dt)_d$, which depends on g, and values obtained from Figures 5*a* and *b* for site 1 are as follows:

g/g_n	$(dD/dt)_d$, in./sec.	$D_d/D_{d,n}$
1.0	1.0	1.0
0.429	0.8	1.43
0.229	0.4	1.71
0.126	0.5	2.38
0.061	0.2	3.06
0.030	0.2	4.38
0.014	0.3	6.65

These values are only approximate because of the difficulty in measuring the slopes of the experimental growth curves. With θ independent of g Equation (3) gives

$$\frac{D_d}{D_{d,n}} = \left(\frac{g}{g_n}\right)^{-1/2}\left[\frac{1 + 0.435(dD/dt)_d}{1 + 0.435(dD/dt)_{d,n}}\right] \quad (3a)$$

Values for $D_d/D_{d,n}$ calculated from Equation (3*a*) are listed in the previous table. The dynamic growth factor in brackets in Equation (3*a*) brings the theory into better agreement with the experimental data as shown in Figure 3. In the low-gravity range the values of $(dD/dt)_d$ become small and fairly constant, and hence Equation (3*a*) reduces to almost a $(g/g_n)^{-1/2}$ variation, which agrees with the trend of the data. From this it appears that the dynamics of bubble growth have an effect on the departure diameter.

Frequency of Single Undisturbed Bubbles

It is first necessary to clearly define the frequency discussed here. For the nucleation sites that were observed the waiting time between the departure of a bubble and the beginning of the next bubble was always zero and consequently does not have to be accounted for in the present calculations. Hence the frequency is defined here as the reciprocal of the growth time for single undisturbed bubbles. It is thus an idealized frequency that would exist if the site were emitting a stream of bubbles, none of which ever coalesced with each other. Actually as described previously there are periods of very high bubble frequency not considered here, where bubbles are being formed and removed from the surface by a large bubble that remains close to the surface because of its low rise rate in reduced gravity.

The ratio of the average frequency in reduced gravity to that for normal gravity is given in Figure 4 [numerical data is given in Table 2(b)] which shows a trend of f decreasing directly with g. This means the bubble growth times generally become much larger when gravity is reduced. Hence with $f \sim g$ and $D_d \sim g^{-1/2}$ the product fD_d is gravity dependent and is approximately proportional to $g^{1/2}$. A correlation presented in (*14*) predicts $fD_d^{1/2} \sim g^{1/2}$ which does not agree with the present information. When the data of $fD_d^{1/2}$ were plotted against g, it was found that for each site there was a tendency for the curves to become less dependent on g as g was reduced. The leveling out appeared to be a function of the heat flux (or ΔT) and implied that the frequency-diameter product becomes less dependent on gravity as the heat flux is increased.

Bubble Growth Rates

When the boiling process is investigated by examining the details of bubble dynamics, a factor of fundamental importance is the rate of growth of bubbles while they are attached to the surface. In the present experiments the water was always at the saturation temperature so that growth and collapse in subcooled liquids were not considered. There are several experiments in the literature on growth rates under normal gravity conditions, and there are a considerable number of mathematical analyses providing growth rate predictions. Since the present work is primarily concerned with the effect of gravity, these references will not be reviewed in detail. The experimental results will be compared with a few of the predictions, and additional information on previous growth rate work can be found for example in (*15*) and (*16*). In general the growth rate predictions have not indicated a gravity dependence (gravity of course has an effect upon the bubble departure time), and one of the objects of the present study was to determine whether or not a gravity dependence is physically exhibited.

Theoretical relations. The growth rate predictions used for comparison are as follows. Fritz and Ende (*17*) considered bubble growth in an infinite uniformly superheated liquid. The heat conduction into the bubble was determined by having the temperature profile in the liquid adjacent to the bubble boundary equal to that for unsteady heat conduction in a slab. Their analysis resulted in the equation

$$D = \frac{4k\,\Delta T}{L\rho v\sqrt{\pi\alpha}}\,t^{1/2} \quad (5)$$

Plesset and Zwick (*18*) included the influence of liquid inertia and accounted for the effect of the spherical shape of the boundary upon the temperature profile, rather than using the temperature distribution in a slab as done by

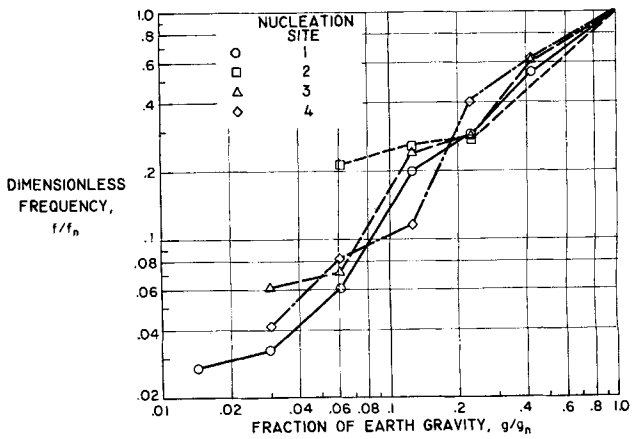

Fig. 4. Effect of reduced gravity on frequency (1/growth time) of single undisturbed bubbles.

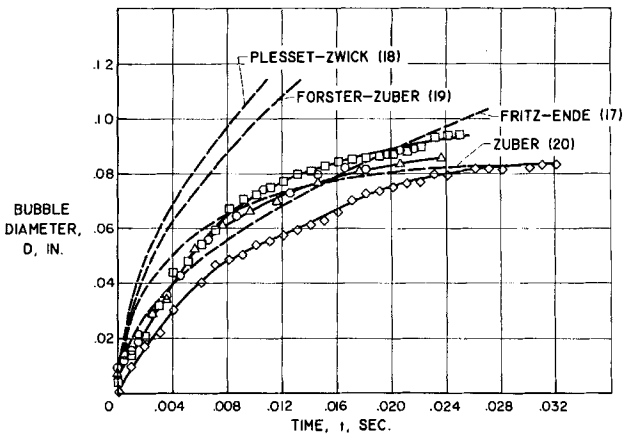

Fig. 5a. Bubble growth data for four typical bubbles in earth gravity, site 1.

Fritz and Ende. This gave the same form as Equation (5) except with a $\sqrt{3}$ introduced on the right side. Forster and Zuber (*19*) obtained the same form as Equation (5) except with a $\pi/2$ included on the right side. Zuber (*20*) considered growth in a nonuniform temperature field and introduced a correction factor for sphericity to obtain

$$D = \frac{\pi}{2}\left[\frac{4k\,\Delta T}{L\rho_v(\pi\alpha)^{1/2}}\,t^{1/2} - \frac{2q_b}{L\rho_v}\,t\right] \qquad (6)$$

All of these expressions were derived for growth in an infinite medium away from solid surfaces. Surface tension, viscosity, and inertia were not considered to be important. Equation (5) indicates a steady increase of diameter with the square root of time, while Equation (6) predicts that a maximum diameter will be reached. More elaborate growth models have been given for example in (*7*), which includes inertia and surface tension for a bubble growing on a surface. The equations must be evaluated numerically, and since this was not carried out in (*7*), it is not known whether the model would provide improved results.

Comparisons for normal gravity. Frist some growth rate curves for normal gravity will be briefly examined. In Figure 5*a* are shown a few curves which are typical of all the data for site 1. For comparison with theory the bubbles selected for measurements were of symmetrical shape and were interfered with as little as possible by preceding bubbles. In Figure 5*a* the Plesset-Zwick and Forster-Zuber predictions are too high. Both the Fritz-Ende and Zuber predictions provide reasonable agreement with the data. However as will be shown later Equation (6) does not seem to apply physically because it predicts that a maximum bubble size will be reached, and this is not found experimentally.

Comparisons for reduced gravity. Considering now the reduced gravity range, growth curves for site 1 have been plotted on Figures 5*b* and *c* [additional data are given in Table 3(b) for site 2]. In the logarithmic plot (Figure 5*c*) the Fritze-Ende relation offers the best general agreement over the entire range of data. However if the data are grouped into initial (< 0.02 sec.) and final (> 0.02 sec.) growth periods, this relation does not indicate the observed diameter variation during the final growth period. The data indicate $D \sim t^{3/8}$ compared with $t^{1/2}$ from theory. In the initial growth period the time exponents were observed to range from 0.5 to 0.8. Staniszewski (*8*) observed that generally the exponent is greater than ½ and sometimes reaches the value of 1 in the early stage of bubble growth; afterwards it decreases with time and in the late stage is approximately 1/3. The total growth time in his experiments was on the order of only 0.030 sec. however which is characteristic of normal gravity bubbles. For all the bubbles observed in the present study the same qualitative behavior was indicated by the data. Usually the decrease in growth rate occurred about 0.010 to 0.020 sec. after initiation of the bubble.

It is interesting to note that for even the longest growth times (0.76 sec.) a maximum bubble size was not attained. In observations of normal gravity bubble growth rates the combination of short cycle times and scatter in measurements could give the impression that a maximum bubble size will be reached (when $dD/dt = 0$); however the very long growth times that occur in low-gravity fields do not substantiate this. In Equation (6) the correction term $-2q_bt/L\rho_v$ causes the bubble to reach a maximum diameter, whereas a maximum is not indicated by the data. In order for the theoretical curve to agree with the data it would be necessary for the maximum in the theoretical curve to occur at a time after the observed bubble detachment. Possibly the quantity q_b should be less than the heat flux q, and not equal to it as assumed in (*20*), and should also be a function of gravity. Equation (6) was derived from a model wherein a superheated liquid layer surrounds the bubble and is pushed upward as the bubble grows (see Figure 8 in reference *20*). The bubble growth is assumed to depend only on the transfer of stored energy which originally is contained in the superheated film. The present bubbles in low gravity become so large that they may grow beyond the superheated layer, and the model used in deriving Equation (6) would not apply. In the final stage of growth the vaporization may occur only around the cylindrical stem at the bubble base. If it is assumed that the heat transfer through the stem area is constant, since the base diameter is fairly constant as shown in Figure 7, then

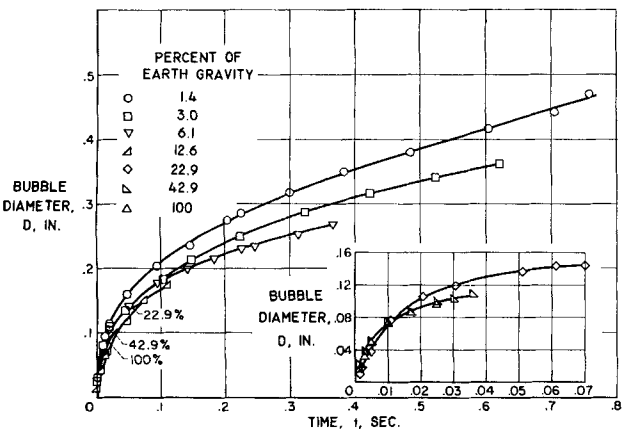

Fig. 5b. Bubble growth data for typical bubbles in seven different gravity fields, site 1.

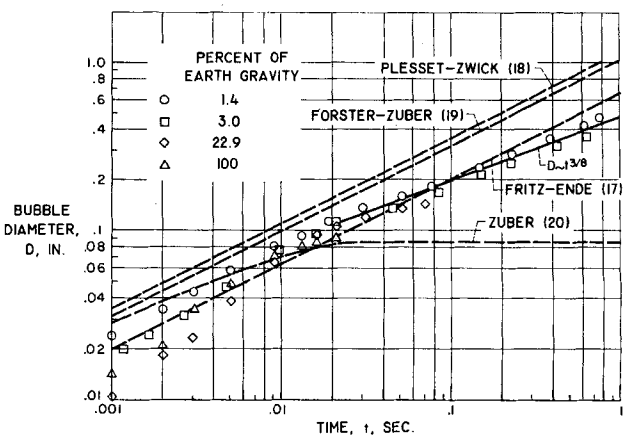

Fig. 5c. Bubble growth data for various gravity fields, site 1.

$$\rho v L \quad \frac{d}{dt}\frac{\pi D^3}{6} = \text{constant}$$

or $D \sim t^{1/3}$*. This is close to the 3/8 power variation indicated by the data in Figure 5c.

The growth analysis in (16) is of interest in that it offers a possibility for introducing a gravity dependence having a physical basis. The theoretical growth in (16) depends on the thickness of a thermal layer of heated fluid adjacent to the surface. In the region of low heat flux the thermal-layer thickness may partly depend on free convection, and hence the layer thickness would be a function of g.

Dynamic Contact Angles

A parameter that may influence bubble departure diameters and growth rates is the time variation of contact angle (dynamic contact angle) between the bubble and the surface while the bubble is growing. In the present investigation contact angle measurements were made during bubble growth for six reduced gravity fields in addition to normal earth gravity. For each data point the contact angle was measured at both sides of the bubble and averaged arithmetically. It was very difficult to make accurate contact angle measurements because extreme clarity and high magnification are required before one can tell whether the actual contact angle at the root of the bubble is being measured rather than the slope of the bubble close to the root. In view of the considerable judgment and interpretation required for these measurements the absolute accuracy is estimated to be within about 10 deg. However since one person reads a given set of data with the same interpretation throughout, the accuracy of readings relative to one another is better. The camera viewed the surface from above at a 5-deg. angle which caused some distortion of the photographed contact angle. However because of the uncertainty in reading the angles accurately it was not felt worthwhile to attempt to correct for this.

Contact angle measurements are shown in Figure 6 for bubbles growing at site 1 in three different reduced gravity fields. [Data for other gravity fields have been omitted for clarity but are tabulated in Tables 3 (a) and (b).] Generally for each bubble the contact angle was found to remain approximately constant during growth, except for short time intervals at the beginning and end of the growth period. In addition for site 1 [Table 3(a)] the contact angle did not vary appreciably with the magnitude of the reduced gravity field. For site 2 [Table 3(b)] the contact angle decreased slightly as gravity was reduced. It was observed that when a bubble begins to detach, a short cylindrical neck is often formed between the bubble and the surface. During this formation the contact angle increases toward 90 deg. This is not shown in Figure 6 because the curvature of a bubble at the surface is often so abrupt that the slope may not be measured accurately.

* Personal communication from Dr. Novak Zuber.

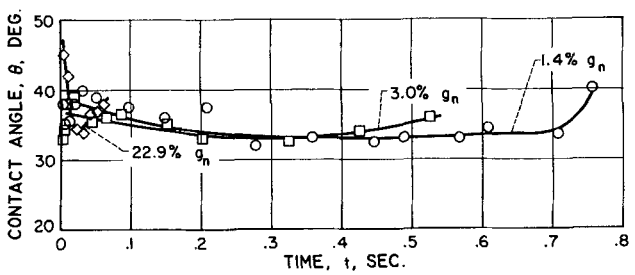

Fig. 6. Contact angle variation during bubble growth at site 1 for three different gravity fields.

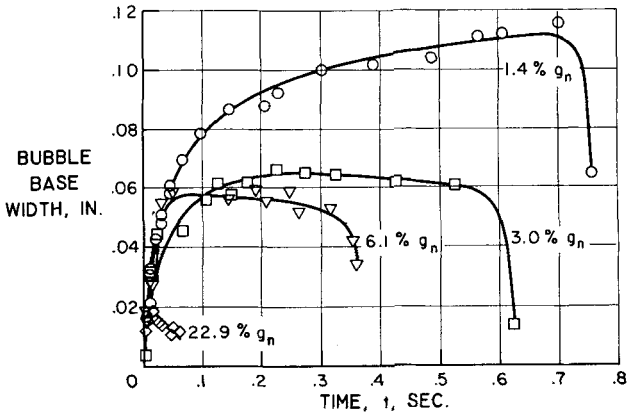

Fig. 7. Bubble base width (contact circle diameter) variation during growth at site 1 for four different gravity fields.

Han and Griffith (7) propose a criterion for departure diameters that is dependent upon the dynamic contact angle. In their experiments the departure size was found to be a function of the receding dynamic contact angle rather than an average contact angle, which is normally used. In their examination of Staniszewski's experiments (8), which indicated a dependence of departure size upon bubble growth rate, they suggest that these apparent dynamic effects upon departure size should instead be attributed to changes in contact angle. In view of the constancy of the contact angle for the very long growth times examined herein it seems more reasonable that contact angle changes are not a cause for departure of the bubble but instead are a consequence of the distortion caused by its impending departure.

Bubble Base Width

The width of the bubble base at the surface (contact circle diameter) was measured during bubble growth at two sites for seven gravity fields, and some of the data for site 1 has been plotted in Figure 7. [Additional information is given in Tables 3(a) and (b).] All of the curves indicate a rapid initial increase in base width. The width does not start from zero in all cases because sometimes there is a small vapor mass left behind when the previous bubble detaches. Throughout most of the growth period the base width remained reasonably constant and then decreased rapidly as the bubble began to detach. In many instances the bubble formed a short cylindrical neck joining it to the surface, and this short vapor column was pinched off (generally not right at the surface) at the instant of departure as shown in Figure 2a. Thus a small vapor mass was left behind which served as a nucleus for the next bubble.

In (16) (see Figure 11 of that reference) the relation between the bubble base width and the bubble height is discussed with respect to the computations in (21). For bubbles up to a range of about 1/16 in. in diameter the results in (21) predict bubble base radii approximately equal to bubble height. The present base sizes are considerably smaller, as illustrated by the normal gravity bubble in Figure 2a.

The previous two sections indicate that the bubbles grow with essentially a constant contact angle and after a short initial period a constant base width. As shown in Figure 2a the growing bubbles were quite spherical in shape for most of the growth period. Hence for the conditions of the present study the bubbles did not fit the model of a spreading hemisphere that is sometimes assumed in theoretical derivations.

Rise Velocity of Detached Bubbles

For site 1 the photographs covered sufficient area so that

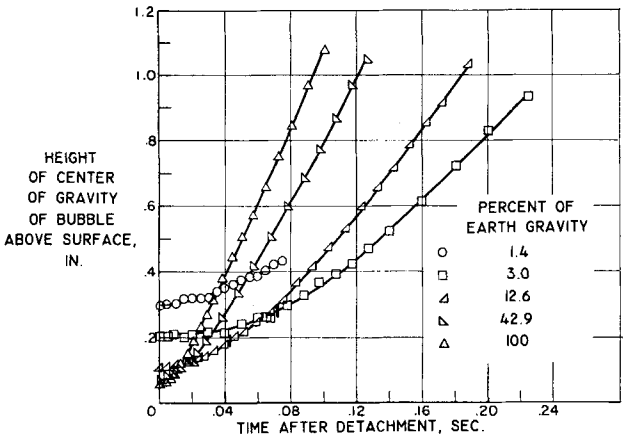

Fig. 8a. Behavior of bubbles after detachment. Rise of center of gravity of bubbles above surface after detachment for five gravity fields, site 1.

bubbles could be followed for about 1 in. of rise from the surface. Bubbles were selected that appeared to have as little interference as possible from other bubbles in the column.

Results for normal gravity. For normal gravity measurements were made for several bubbles, and one typical path which gives the height of the center of gravity above the surface as a function of time is shown in Figure 8*a*. After the bubble has moved upward about 0.7 in. the slope of each such curve becomes constant and gives a freely rising velocity (listed in Table 4). The velocities for normal gravity were in the range from 11.3 to 12.1 in./sec. An equation in (22) for moderately distorted ellipsoidal bubbles gives

$$u_\infty = 1.53 \left[\frac{\sigma_{lv}\, g\,(\rho_l - \rho_v)}{\rho_l^2} \right]^{1/4} \qquad (7)$$

This predicts a u_∞ of 9.41 in./sec. for normal gravity, which is somewhat less than the measured values.

Results for reduced gravity. Some bubble paths for reduced gravity are illustrated in Figure 8*a*. The vertical line drawn through some of the curves gives the time after which no more bubbles generated at the surface coalesce with the rising bubble. For 0.014 g_n the coalescence process had not been completed when the run ended. Velocities measured from the slopes at the upper ends of the curves are given in Figure 8*b* as a function of gravity (tabular values are in Table 4). Equation (7) indicates that $u_\infty/u_{\infty,n} \sim (g/g_n)^{1/4}$, and this is in very good agreement with the data except at the lowest gravity. For this gravity it was not possible to follow the bubble very far before the low-gravity period ended because of its slow rate of rise, and hence the bubble had not accelerated to its final steady velocity.

CONCLUDING REMARKS

One of the most notable observations of the effects of reduced gravity on bubble dynamics was the very rapid removal of small vapor bubbles from the boiling surface by a previously detached bubble that momentarily remained just above the surface because of its slow rise rate and thus serves as a temporary vapor reservoir. Nucleation from a single site in low gravity consisted of the generation of one large bubble, then several small bubbles of high frequency that are absorbed by the large bubble, and then a large bubble again. The rapid absorption of the small bubbles helps to maintain a high turbulence level near the surface so that as the gravity field is reduced the heat transfer coefficients may still remain high.

For the single bubbles measured herein it was found that the diameters at departure increased approximately as $g^{-1/3}$ for fields between 0.1 and 1 g_n and for lower gravities increased as $g^{-1/2}$. The latter is the functional relation predicted from considering a balance of surface tension and buoyancy forces at departure. The inclusion of a dynamic term as suggested by Staniszewski (8) provided a moderately improved correlation.

The results for the frequency-diameter product at departure were much more scattered than the departure diameters. There was a general trend of fD_d to decrease as gravity was reduced and then tend to become fairly constant below a certain gravity. The gravity at which the curve became more nearly constant increased with q, so that for higher q's it is possible that fD_d may become independent of gravity.

In reduced gravity the bubbles become quite large, and the growth times are long compared with those in earth gravity. The bubble size increases continuously, in accordance with the approximate relation $D \sim t^n$ where $n = 0.5$ to 0.8 for $t < 0.02$ sec. and $n \approx 3/8$ for $t > 0.02$ sec. The growth curves can be approximated fairly well by a $t^{1/2}$ behavior, but this does not reveal that the growth rate is actually much more rapid during the initial stages than during the final stages.

The bubble contact angle was found to be essentially independent of gravity. Also during the relatively long growth periods for reduced gravity the contact angle remained substantially constant except during a short initial period and near bubble departure. The larger bubbles in reduced gravity were accompanied by larger base widths (contact circle diameters).

The rise velocity of bubbles after departure approaches a steady value after the bubble has moved about 0.7 in. from the surface. This value is a function of gravity and was found to agree well with theory predicting $u_\infty \sim g^{1/4}$.

The preceding results are all for individual bubbles formed on a flat horizontal surface in distilled water. For a more viscous liquid the drag and dynamic forces may have a different relation to the buoyancy force, and hence the behavior in reduced gravity could be considerably different than the present results. Some preliminary experiments have exhibited this and will be the subject of future study.

NOTATION

c_p = specific heat at constant pressure
D = bubble diameter
f = bubble frequency
g = gravitational field
k = thermal conductivity
L = latent heat of vaporization
q = heat transferred per unit area and time from solid surface to liquid

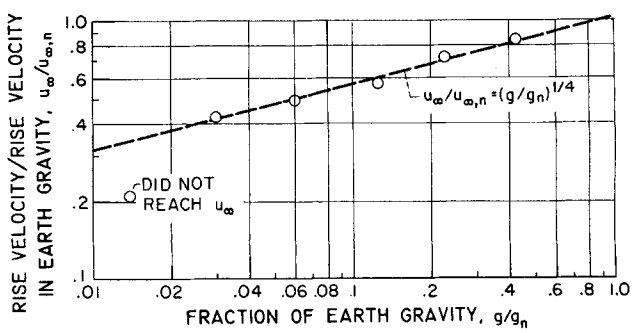

Fig 8b. Behavior of bubbles after detachment. Effect of gravity field on velocity of freely rising bubbles for earth gravity, $u_{\infty n}$ = 11.8 in./sec.

q_b = heat transferred per unit area and time from vapor within a bubble to bulk liquid
T = temperature; T_w = surface temperature; T_{sat} = saturation temperature
ΔT = temperature difference, $T_w - T_{sat}$
t = time
u_∞ = rise velocity of bubble far from boiling surface
α = thermal diffusivity, $k/\rho c_p$
θ = contact angle between bubble and surface
ρ = density
σ = surface tension

Subscripts

d = at detachment
l = liquid
n = normal (earth) gravity
v = vapor

LITERATURE CITED

1. Merte, H., Jr., and J. A. Clark, *J. Heat Transfer*, **83**, No. 3, pp. 233-242 (1961).
2. Costello, C. P., and W. E. Tuthill, *Chem. Eng. Progr. Symposium Ser. No. 32*, **57**, (1961).
3. Graham, R. W., and R. C. Hendricks, Nat'l. Aeronaut. and Space Admin. *Tech. Note D-1196* (1963).
4. Ivey, H. J., *AEEW-R99* (Sept., 1961).
5. Usiskin, C. M., and R. Siegel, *J. Heat Transfer*, **83**, No. 3, pp. 243-253 (1961).
6. Zuber, N., Ph.D. thesis, Univ. Calif., Berkeley, California (June, 1959).
7. Han, Chi-Yeh, and P. Griffith, *Rept. 7673-19*, Dept. Mech. Eng., Mass. Inst. Technol., Cambridge, Massachusetts (Mar., 1962).
8. Staniszewski, B. E., *Tech. Rept. 16*, Div. Sponsored Res., Mass. Inst. Technol., Cambridge, Massachusetts (Aug., 1959).
9. Siegel, R., and C. M. Usiskin, *J. Heat Transfer*, **81**, No. 3, pp. 230-236 (1959).
10. Siegel, R., *Trans. Am. Soc. Mech. Engrs.*, **80**, 347-359 (1958).
11. Moissis, R., and P. J. Berenson, *Am. Soc. Mech. Engrs. Paper 62-HT-8* (Aug., 1962).
12. Fritz, W., *Phys. Zeit.*, **36**, 379 (1935).
13. Cole, Robert, *A.I.Ch.E. Journal*, **6** (Dec., 1960).
14. McFadden, P. W., and P. Grassman, *Int. J. Heat and Mass Transfer*, **5**, 169-173 (1962).
15. Strenge, P. H., A. Orell, and J. W. Westwater, *A.I.Ch.E. Journal* **7**, 578-583 (1961).
16. Hsu, Y. Y., and R. W. Graham, Nat'l. Aeronaut. and Space Admin. *Tech. Note D-594* (1961).
17. Fritz, W., and W. Ende, *Phys. Zeit.*, **37** (1936).
18. Plesset, M., and J. A. Zwick, *J. Appl. Phys.*, **25**, 493 (1954).
19. Forster, H. K., and N. Zuber, *ibid.*, p. 474.
20. Zuber, N., *Int. J. Heat and Mass Trans.*, **2**, 83-98 (1961).
21. Bashforth, F., and J. C. Adams, "An Attempt to Test Theories of Capillary Action by Comparing the Theoretical and Measured Forms of Drops of Fluid," p. 80, Cambridge Univ. Press, England (1883).
22. Harmathy, Tibor, *A.I.Ch.E. Journal*, **6**, 281 (1960).

Manuscript received July 24, 1963; revision received November 26, 1693; paper accepted November 27, 1963. Paper presented at A.I.Ch.E. San Juan meeting.

Turbulent Disruption of Flocs in Small Particle Size Suspensions

DAVID G. THOMAS

Consultant to Aerojet-General Nucleonics, San Ramon, California

In the absence of turbulent fluctuations the main effect of a velocity gradient on the floc properties is a rearrangement of particles within the floc producing a more dense floc structure. When the suspension is sufficiently dilute that floc-floc collisions are negligible, the limits on the floc diameter are $(1 + \alpha)^{5/3} < (D_f/D_p) \leq (1 + \alpha)^2$, where α is the ratio of the volume of fluid immobilized in the floc structure to volume of solids in the floc structure as determined from hindered-settling measurements. These results set an upper limit on the floc size.

Under turbulent flow conditions the principle mechanism leading to floc rupture is pressure differences on opposite sides of the floc which cause bulgy deformation and rupture. The breakup of the floc is resisted by the yield stress τ_y and is promoted by an increase in the energy dissipation per unit mass of fluid ϵ. Because the energy dissipation per unit mass is at a maximum near the pipe wall, the floc size is at a minimum in this same region.

By application of the concepts of local isotropy, the floc size is found to be proportional to $(\tau_y^9/\epsilon^5)^{1/2}$ once the turbulent intensity is sufficient to overcome the yield stress. In the wall region the floc diameter is proportional to $(du/dr)^3\ (\tau_y^9/\epsilon^8)^{1/2}$.

The hydrodynamic splitting of liquid drops suspended in immiscible liquids has been the subject of many theoretical and experimental studies (*1* to *4*). As a result the factors responsible for a given drop size distribution are rather well defined. In contrast to this the dynamics of the disruption of clumps of flocculated solid particles has received little attention, even though the agglomeration process has been studied in detail (*5*, *6*). One reason for this may be the intangible nature of the floc. (A floc may be considered as a loose, irregular, three-dimensional cluster

David G. Thomas is with the Oak Ridge National Laboratory, Oak Ridge, Tennessee.